Composites Part B 238 (2022) 109880

Contents lists available at ScienceDirect

Composites Part B

journal homepage: www.elsevier.com/locate/compositesb

Dual-mode biomimetic soft actuator with electrothermal and magneto-responsive performance

Wenwen Li [a], Min Sang [a], Shuai Liu [a], Bochao Wang [a], Xufeng Cao [a], Guanghui Liu [c,d], Xinglong Gong [a,b,*], Lingyun Hao [d], Shouhu Xuan [a,b,**]

[a] CAS Key Laboratory of Mechanical Behavior and Design of Materials, Department of Modern Mechanics, University of Science and Technology of China, Hefei, Anhui, 230027, PR China
[b] State Key Laboratory of Fire Science, University of Science and Technology of China, 96 Jinzhai Road, Hefei, Anhui, 230026, PR China
[c] School of Energy, Materials and Chemical Engineering, Hefei University, 99 Jinxiu Avenue, Hefei, 230601, PR China
[d] School of Materials Engineering, Jinling Institute of Technology, Nanjing, 211169, PR China

ARTICLE INFO

Keywords:
Actuator
Electrothermal
Magnetic
Thermal management
MXene

ABSTRACT

Soft actuators with large deformation and high stability in response to multi-stimuli are highly demanded in biomimetic applications. However, most of the present actuators driven by a single stimulus often exhibit low performance and high energy consumption. In this work, a sandwich structural soft actuator (MPDMS/MXene/PTFE) which possesses electrothermal/magnetic coupling actuation is fabricated by combining magnetic NdFeB/Polydimethylsiloxane (MPDMS) composite layer, MXene film, and PTFE tape together. Due to the large difference of thermal expansion coefficient between MPDMS film and PTFE tape, the soft actuator shows a wonderful electrothermal actuation and the bending deformation can reach to as high as 353° under a 3 V power supply. The excellent electrical conductivity of MXene component endows the sandwich film with good thermal management performance, thus the soft MPDMS/MXene/PTFE sandwich films can be applied in the thermal treatment of body and thermal imaging. Most importantly, the soft actuator also exhibits a typical magnetic biomimetic actuation and the programmable actuation performance of the dragonfly actuator can be demonstrated by both experiments and finite element simulations. Eventually, the electrothermal/magnetic coupling actuation is successfully applied in an intelligent crawling robot to overcome the traditional inchworm movement simulation.

1. Introduction

Soft robots have attracted increasing attentions in medical care [1], goods transportation [2], and intelligent artificial robots [3] because they can produce desirable deformation under different external stimuli such as electricity [4,5], magnetism [6–8], humidity [9–11] and light [12–14]. The electrically driven actuators have the advantages of simple operation, easy storage and use, and strong controllability, thus they possess wide potential in AI systems. During the past decades, electroactive polymer actuators (EAPs), mainly ionic or field-activated polymers, have been extensively studied because of their low weight, large deformation, flexibility and low cost [15]. However, the actuations mostly occur only in electrolyte solutions, which are inconvenient for practical application because of the requirement of high-standard safety encapsulation of the liquid electrolyte. Moreover, in the field-activated classification, dielectric elastomers typically require high applied electric fields, which also severely restricts their applications [16]. To this end, more energetic soft actuators with diverse driving performance are highly required to meet the quickly improved instrumented environment.

Electrothermal actuators, based on the difference of thermal expansion coefficient of two materials, have been actively studied due to the advantages of light weight, electrolyte-free and simple excitation [17,18]. It was reported that the graphene [19,20], carbon nanotubes

* Corresponding author. CAS Key Laboratory of Mechanical Behavior and Design of Materials, Department of Modern Mechanics, University of Science and Technology of China, Hefei, Anhui, 230027, PR China.
** Corresponding author. CAS Key Laboratory of Mechanical Behavior and Design of Materials, Department of Modern Mechanics, University of Science and Technology of China, Hefei, Anhui, 230027, PR China.
E-mail addresses: gongxl@ustc.edu.cn (X. Gong), xuansh@ustc.edu.cn (S. Xuan).

https://doi.org/10.1016/j.compositesb.2022.109880
Received 9 February 2022; Received in revised form 30 March 2022; Accepted 7 April 2022
Available online 11 April 2022
1359-8368/

[21] and metal nanowires [22] could be applied as the conductive layers in preparing electrothermal actuators. Recently, Lee et al. [23] reported a Ag nanowire-based directional transparent shape morphing (ATSM) actuator, which showed a high deformation (2.5 cm^{-1}) under 40 °C. The actuator was a transparent trilayered composite with giant linear coefficient of thermal expansion (CTE) mismatch with an integrated highly transparent and flexible silver nanowire (AgNW) percolation network heater. Because of the light weight and large deformation, biomimetic robots based on the electrothermal drive have been widely studied. Kim et al. reported various color-shifting biomimetic soft robots, such as color-shifting blooming flower and fluttering butterfly [24]. Recently, Hu et al. have developed biomimetic inner spiral arm for pulling objects out of pipes and artificial snake capable of deformation and color-change simultaneously, based on paper-based electrothermal drives [25]. Originated from the remarkable electrical conductivity, layered structure and abundant surface chemistry [26,27], MXene shows a good prospect in the field of electromagnetic interference shielding [28], sensors [29,30] and soft actuators [31]. By integrating the MXene and low-density polyethylene composite together, a bilayer-structure actuator with multi-responsive characteristics was developed. Typically, the actuator showed a large offset distance (20 mm) with a driving electric voltage as low as 1.5 V, and the corresponding curvature and temperature reached to 0.079 mm^{-1} and 32.7 °C, respectively [32]. However, with the improvement of AI, the practical environments become more and more complex, the traditional electrothermal actuators driven by the single electrical stimulation limit their wide application. Therefore, it is urgent to develop high-performance actuators that can respond to multiple stimuli.

Recently, multi-responsive actuators driven by electricity and humidity [11,33], electricity and light [34], electricity and heat [35] have been intensively studied. It is reported that the SRGO/PI double-layer actuator could convert both electrical and optical stimuli into heat, thus the bending deformation accompanied by large and rapid actuation were easily achieved [34]. Specifically, the magnetically induced actuators have advantages of wireless actuation, remote control, and non-contact with the actuators, thus they received wide research interests [36,37]. To date, considerable progress has been made in verifying the driving mechanism of magnetic actuators. Typically, the magnetic-driven soft actuators with programmable magnetized profiles have been easily fabricated by modulating the magnetic dipole arrangement in the composites [38–40]. Recently, Zhao et al. have further introduced two kinds of magnetic particles, Fe_3O_4 and NdFeB, into shape memory polymers [41]. Under 1.5 T pulsed magnetic field, the deformation of the composite could be programmed, and it could selectively grasp heavy objects or complete the structural deformation of the antenna. Obviously, the coupling of magneto-actuation with other stimuli-responsive functions attracts an increasing attention. Kyungchan et al. reported a polymer electroactive actuator, which could be promoted by a significantly low driving voltage (<0.5 V) in the presence of an external magnetic field, thus had a very large swinging speed [42]. Recently, Zhang et al. studied the driving characteristics of the composite structure of electroactive polymer and magneto-elastomer by experiment and finite element analysis, and proved that the coupling drive of electric and magnetic field could realize double deformation in Origami folding [43]. In consideration of the easy operation of the electrothermal actuation, the combination of electrical stimulation and magnetic stimulation is rarely applied to soft actuators. Therefore, a dual-mode soft actuator is developed to further improve the driving performance of the actuator, which can also expand the application of the actuators.

This work develops a multifunctional MPDMS/MXene/PTFE soft actuator, which presents both electrothermal and magneto-actuated deformation behaviors. The MPDMS/MXene/PTFE shows an excellent electric conductivity thus the hybrid film shows wide applications in heat therapy and thermal imaging. Due to the difference in thermal expansion coefficient of the MPDMS and PTFE layers, the sandwiched film exhibits a typical electrothermal actuation performance and the as-prepared gripper device serves well in transporting the target object. In addition, the MPDMS/MXene/PTFE actuator has dual-mode response under magnetic field due to the magnetic nature of MPDMS layer. Based on this characteristic, a biomimetic dragonfly actuator is prepared and the programmability of the actuator is verified by experiment and finite element simulation. Finally, an intelligent crawling robot is developed to simulate the movement of Inchworm by utilizing the unique electrothermal-magnetic coupling actuation. These studies provide new ideas for the design of high-performance soft actuators towards various practical applications, such as smart devices, soft robotics, artificial muscles and wearable soft electronics.

2. Experiments and characterization

2.1. Materials

Ti_3AlC_2 MAX powder (400 mesh size) was purchased from 11 Technology Co., Ltd, Jilin, China. Lithium fluoride (LiF) was bought from Aladdin Chemical Co., Ltd, China. The concentrated hydrochloric acid (HCl) was provided by Sinopharm Chemical Reagent Co., Ltd, Shanghai, China. The polytetrafluoroethylene (PTFE) tape was commercially available product, China. The polydimethylsiloxane (PDMS) precursor and curing agent (Sylgard 184) were obtained from Dow Corning. The NdFeB particles (size 5 μm) were purchased from Guangzhou Nuode Transmission Parts Co., Ltd, China. All reagents were used without further purification and distilled water was used.

2.2. Fabrication of MPDMS/MXene/PTFE sandwich film, soft actuator and four-finger soft actuator

Synthesis of MXene nanosheets: $Ti_3C_2T_X$ nanosheets were prepared according to the previously reported method by selectively etching the Al layer from the precursor of MAX phase (Ti_3AlC_2) with LiF/HCl solution [44]. Typically, LiF (1 g) was dissolved in HCl solution (20 mL, 9 M) in a Teflon beaker and stirred at 200 rpm for about 30 min at room temperature, and then Ti_3AlC_2 MAX precursor (1 g) was slowly added under constant magnetic stirring. After the mixture was stirred at 35 °C for 24 h, the resulting black slurry was repeatedly washed with deionized water until the pH of the supernatant exceeded 6. The black swelled clay-like sediment was dispersed in deionized water, followed by continuous ultrasound for 1 h in an ice bath, and then centrifuged at 3500 rpm for 1 h. The supernatant after centrifugation was $Ti_3C_2T_X$ (MXene) nanosheets.

MPDMS/MXene/PTFE soft actuator and four-finger soft actuator: Firstly, MPDMS magnetic films were synthesized by the spin-coating process. 15 g PDMS and 4.125 g (20 wt%) NdFeB powder were weighed in a three-mouth flask and stirred at a speed of 200 rpm for 1 h. Then 1.5 g crosslinking agent was added, and the PDMS/NdFeB mixture was obtained after stirring for 15 min. Subsequently, 1.5 mL PDMS/NdFeB mixture was poured on a silicon wafer for spin-coating. After that, the spin-coated silicon wafer was placed in a large magnetic field, solidified and magnetized at 90 °C for 15 min under the magnetic field of 1000 mT to obtain MPDMS magnetic films. Pure MXene film was fabricated by vacuum-assisted filtration. Then, the PTFE/MXene double-layer structure was obtained by placing the self-adhesive PTFE tape on one side of the pure MXene membrane. Finally, an ultra-thin layer of PDMS was coated on the MXene/PTFE film. After that, the magnetic MPDMS film was pasted on the above film and cured at 50 °C for 3 h to generate MPDMS/MXene/PTFE sandwich film. The four U-shaped actuators were fabricated using the process mentioned above. A cross-shaped PET film and a 3D-printed stand were used to hold the four-finger gripper. The tail of the four soft actuators was glued together with silver adhesive on copper foil, and then it was fixed on PET film with double-sided adhesive while the other ends of the actuators could be bend freely.

2.3. Characterizations

The surface morphology of MXene film and the cross-sectional morphologies of MXene film, PTFE tape and MPDMS/MXene/PTFE sandwich structure were characterized by scanning electron microscopy (SEM, Sirion 200) equipped with an energy-dispersive spectroscopy (EDS) system. The transmission electron microscopy (TEM) images of MXene nanosheets were recorded by field-emission transmission electron microscopy (FETEM, JEM-2100F). The height morphology of MXene nanosheet was characterized by the atomic force microscope (AFM, dimension icon, Bruker). The crystalline phase of Ti_3AlC_2 powder and MXene film were identified by X-ray diffraction (XRD, SmartLab, Japan). X-ray photoelectron spectroscopy (XPS) of the products was shown on applied electron spectrometers (ESCALAB 250). The mechanical properties of MPDMS/MXene/PTFE sandwich structure were tested by the Materials Test System (MTS). The electrothermal performance of MPDMS/MXene/PTFE sandwich structure was explored by an auto range DC power supply (IT8500, Itech electronic Co., Ltd) and a thermocouple device (DT-3891G, Shenzhen Everbest Machinery Industry Co., Ltd, China) with a multiple datalogger data analysis software. Infrared electrothermal images were recorded by an infrared camera (ImageIR 8325). The thicknesses of MXene film, MPDMS film, PTFE tape and MPDMS/MXene/PTFE sandwich structure were measured by a digital micrometer (Sanliang Corporation, 0–25 mm). The hysteresis loops of the materials were tested by HyMDC (Hysteresis Measurement of Soft and Hard Magnetic Materials). The finite element simulation was calculated by COMSOL software.

3. Results and discussion

3.1. Preparation and characterization of MXene film and MPDMS/MXene/PTFE sandwich film

Fig. 1 shows the schematic illustration for the preparation of MPDMS/MXene/PTFE sandwich films with electrothermal and magnetic coupling actuation characteristics. Firstly, the $Ti_3C_2T_X$ nanosheets are prepared by selectively etching the Al layer from the precursor of MAX (Fig. 1). As shown in Fig. 2a, the MXene aqueous solution shows a remarkable Tyndall effect, indicating its typical colloidal characteristic and good dispersibility. As confirmed by TEM image (Fig. 2b), the MXene nanosheet shows a thin laminated structure. After the etching process, the characteristic peak (104) of Ti_3AlC_2 powder at $2\theta \approx 39^\circ$ disappears (Fig. 2c) which demonstrates that the Al layer has been completely removed and the MXene is successfully obtained. Furthermore, in comparison to the Ti_3AlC_2 powder, the (002) peak of MXene shifts to smaller angles (9.44°–6.14°), suggesting that the interspace between MXene flakes has been enlarged. The AFM images (Fig. 2d and e) verify that the MXene presents a 2D layered structure with a thickness of about 1.5 nm, demonstrating that few-layer of MXene sheets have been successfully synthesized. XPS analysis has been employed to further investigate the chemical compositions of MXene flakes (Fig. 2f). The clear signals of Ti, C, O, and F elements indicate that the few-layered MXene flakes are successfully exfoliated from the MAX. In this work, the MXene solution was filtered on the filter membrane to prepare MXene film with several layers thickness. As shown in Fig. 2g, the resulting MXene film has a rough and wrinkled surface. Furthermore, the vacuum-filtrated MXene film exhibits an ordered lamellar structure with many interlayer gaps (Fig. 2h). The elemental mapping images of the cross-section of MXene film are presented in Fig. 2i to disclose the element composition and spatial distribution. Clearly, C, O, F and Ti elements are evenly distributed throughout the MXene film, which demonstrates the compact nanostructure of the final product.

Since the MPDMS/MXene/PTFE sandwich structure can be tailored at will, it is easy to fabricate U-shaped soft actuators (Fig. S1). Fig. 3a displays the thin film and U-shaped soft actuator based on the MPDMS/MXene/PTFE sandwich structure. Fig. 3b shows the SEM image of cross-section of the MPDMS/MXene/PTFE sandwich film. The three-layer structure is clearly observed. The thicknesses of the MPDMS, MXene, and PTFE layers are measured to be 60, 14, and 80 μm, respectively. Besides, the commercially available PTFE tape has a high-temperature resistant adhesive layer, thus the PTFE tape exhibits a double layer structure (Figs. S2 and 3b). Here, the adhesive gel enable the PTFE be strongly bonded to the MXene film.

The tensile test of MPDMS/MXene/PTFE sandwich film (0.5 × 2.9 cm^2) was carried out to characterize its mechanical properties by Materials Testing System (Fig. 3d). The tensile stress-strain curves are recorded in Fig. 3f and Fig. S3a and b. The MXene film and MPDMS film both undergo a stage of elastic deformation until finally fracture. The MPDMS film possesses the smallest tensile strength of 1.88 MPa and elongation of 136% at break. The MXene film has the maximum tensile strength of 34.85 MPa, but its elongation at break is up to 0.776%. For the PTFE tape, it is in the linear elastic stage at the initial stage and its

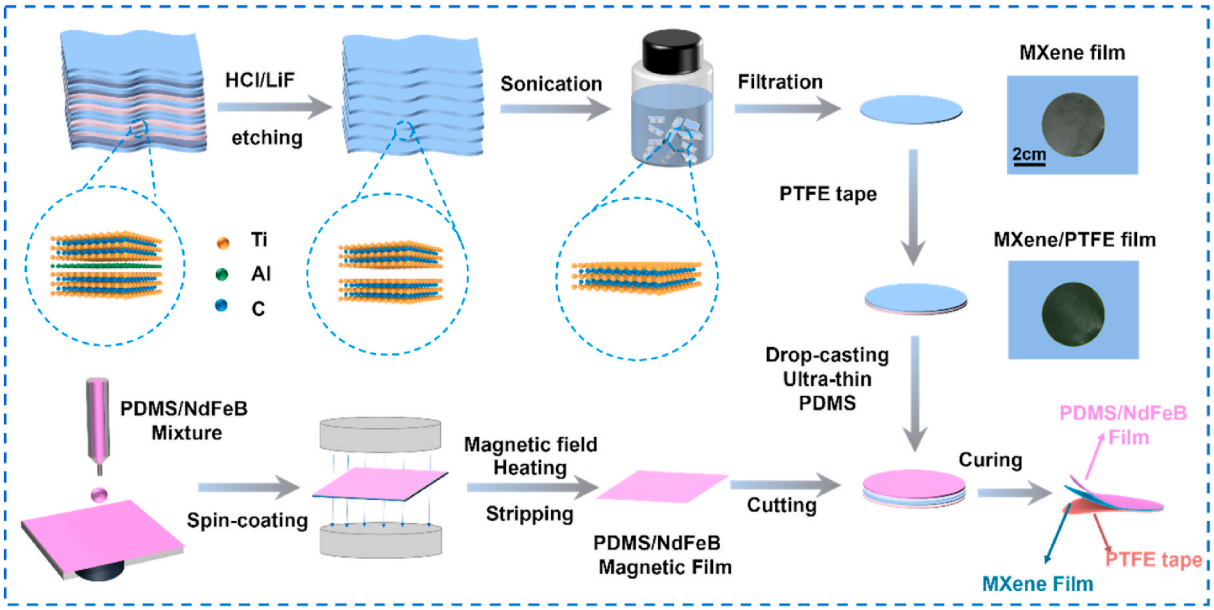

Fig. 1. Schematic of the fabrication process of (a) MXene film and (b) MPDMS/MXene/PTFE sandwich structure.

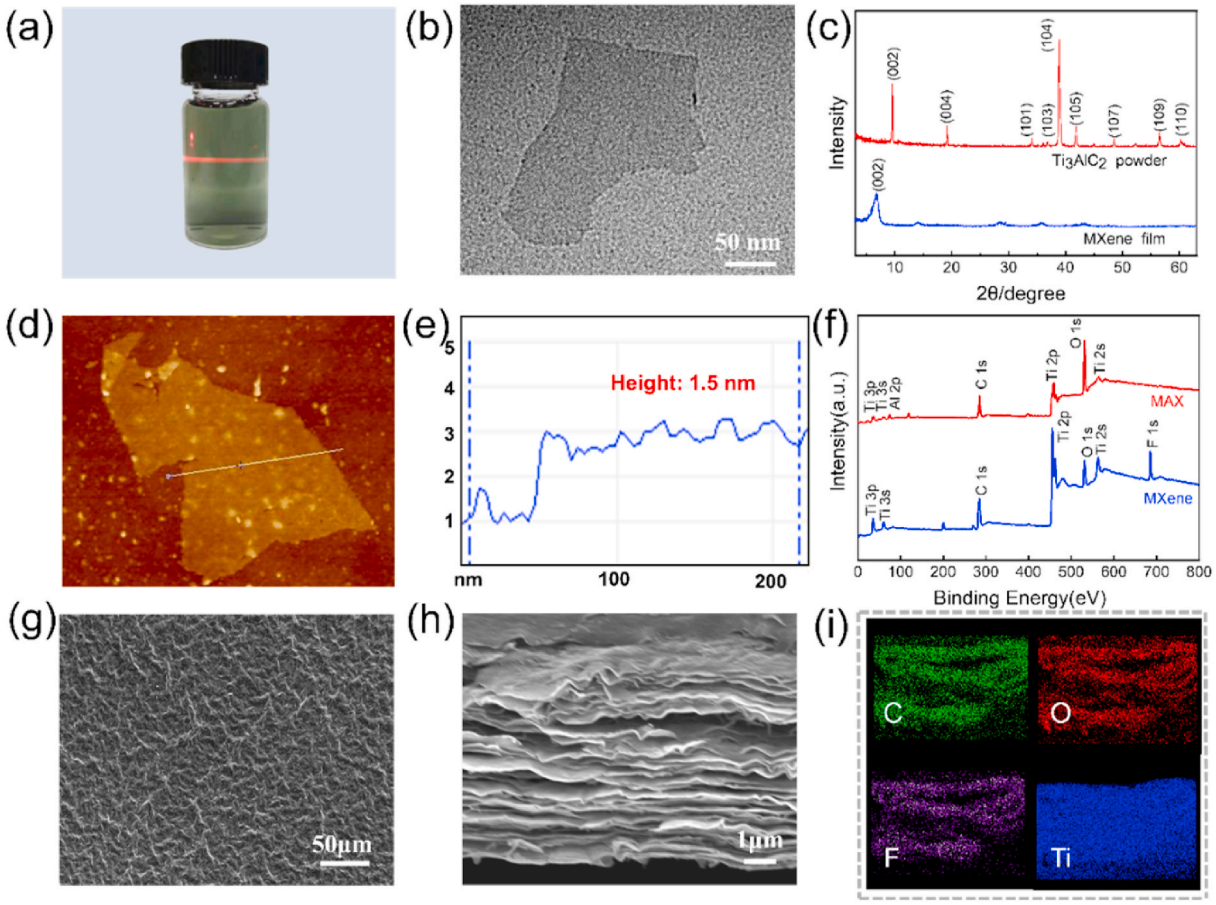

Fig. 2. (a) Optical image of MXene suspension. (b) TEM image, (d) AFM image and (e) height morphology of MXene nanosheets. (c) XRD patterns and (f) XPS spectra of Ti_3AlC_2 powder and MXene film. (g) SEM image of MXene film surface. SEM images of (h) the cross-section and (i) the corresponding elemental mapping image of MXene film.

stress increases with strain. When the yield point is reached (5.12 MPa), at which necking is generated, it shows a significant stress reduction. Subsequently, the necking gradually expands while the stress remains stable, until the test area is fully necked. This process must be corresponding to the clod drawing stage. Here, the material enters the hardening area and the stress gradually increases until fracture (7.43 MPa) as the stretching progresses. As shown in Fig. S3c, the stress-strain curve of MXene/PTFE double-layer structure is similar to that of PTFE tape, and its maximum tensile strength is 5.27 MPa and the elongation at break is 344.5%. Therefore, the MPDMS/MXene/PTFE sandwich structure possesses the tensile strength of 4.59 MPa and elongation of 435.8% at break. As shown in Fig. 3g, the MPDMS/MXene/PTFE sandwich structure shows two fracture points in the stress-strain curve. The first breaking point is attributed to the MPDMS film and the second is caused by the simultaneous breaking of the PTFE tape and the MXene film. The good mechanical properties ensure the sandwich film be more stable and durable during the heating drive process. Furthermore, Fig. 3h shows the M − H curve of NdFeB particles and MPDMS film. With increasing of magnetic field, the magnetization increases and eventually saturates. The magnetization curves are essentially not coincident with the demagnetization one, which exhibit the typical hard magnetic properties. In this case, the maximum magnetization of the 20 wt% MPDMS film is 17.9 emu g^{-1}.

3.2. Electrothermal characteristics of MPDMS/MXene/PTFE soft actuator

Owing to the conductive MXene, the MPDMS/MXene/PTFE sandwich film possesses a good electrothermal behavior. Therefore, a U-shape MPDMS/MXene/PTFE soft actuator with a unique electrothermal characteristic can be prepared by a simple "tape and cut" method (Fig. 4a). The electrical conductivity of the MPDMS/MXene/PTFE U-shape soft actuator was first studied. As shown in Fig. 4b, the soft actuator can successfully light a heart lamp, which indicates the conductivity of MXene film is high (Fig. S4). Fig. 4c displays the steady real-time relative electrical resistance of the U-shaped soft actuator, the results demonstrate that the soft actuator shows a high electrical stability. Here, due to the famous Joule effect, the MPDMS/MXene/PTFE sandwich film has a wonderful electrothermal property. Fig. 4d exhibits the time-dependent temperature curves of the MPDMS/MXene/PTFE soft actuator at different voltages. When the voltage is turned on, the temperature of the actuator rises rapidly until the steady state temperature is reached. When the voltage is turned off, the temperature drops rapidly to room temperature. The temperature of the U-shaped soft actuator can reach about 110 °C at a voltage of 3 V. As a heating actuator, its reliability, stability and repeatability are vital in practical applications. The temperature change over a long time at a constant voltage of 2.5 V is recorded to evaluate the long-term heating stability of MPDMS/MXene/PTFE soft actuator (Fig. 4e). The temperature of the actuator basically remains unchanged even after loading external voltage over 2400 s, confirming the long-term heating stability. Furthermore, after 40 lift-cooling switching cycles, the actuator still maintains stable electrothermal performance (Fig. 4g). Besides, the saturation temperature of MPDMS/MXene/PTFE soft actuator can be precisely adjusted according to the real-time variation of voltage (Fig. 4f) and the temperature gradually increases with the input voltages, which is also recorded by an

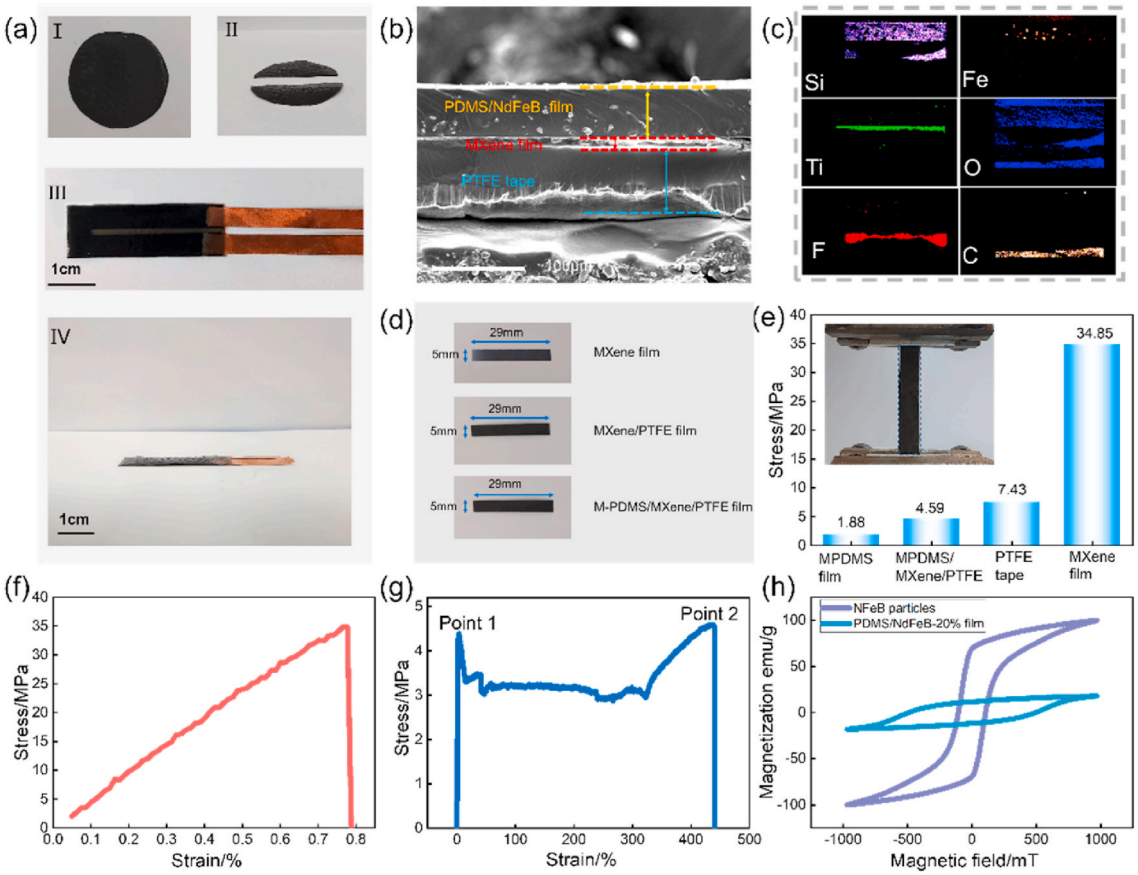

Fig. 3. (a) Optical image of the MPDMS/MXene/PTFE sandwich structure and the U-shaped actuator. (b) SEM image and (c) the corresponding elemental image of the cross-section of MPDMS/MXene/PTFE sandwich structure. (d) Optical image of mechanical test sample. (e) The tensile strength of MPDMS film, MPDMS/MXene/PTFE sandwich structure, PTFE tape and MXene film. The tensile stress–strain curves of (f) MXene film and (g) MPDMS/MXene/PTFE sandwich structure. (h) Magnetic hysteresis loops for NdFeB particles and 60 μm-thick MPDMS film with 20 wt% NdFeB particles.

infrared radiation thermal imaging camera (Insert of Fig. 4f). In addition, it can be observed in Fig. 4h that a linear relationship can be fitted between the saturation temperature and the input power density. The saturation temperature increases with increasing input power, and thus the deformation of the soft actuator can be programmatically controlled.

The actuation of the electrothermal actuator is based on the strain mismatch of two materials with different thermal expansion coefficients when the temperature rises. The MPDMS/MXene/PTFE soft actuator is composed of three layers including MPDMS film, MXene film, and PTFE tape. As shown in Fig. 5a, When the circuit is connected, the temperature of PTFE tape and MPDMS film increases. Due to the different thermal expansion of PTFE tape ($355.9 \times 10^{-6}\ K^{-1}$) and MPDMS film ($-269 \times 10^{-6}\ K^{-1}$), the soft actuator curves. A good electrothermal soft actuator requires the following features: (1) The two driving layers should have different thermal expansion coefficient; (2) The material as heating layer requires high electrical conductivity, thus can produce a high temperature upon low voltage. Meanwhile, it can provide good and stable heating performance during the actuating process; (3) All materials should be stable over a wide temperature range. In this work, the electrical conductivity of MXene film is high and the difference of thermal expansion coefficient between MPDMS film and PTFE tape is large, thus they are selected as the heating layer and the driving layer, respectively.

With increasing of the applied voltage, the bending angles of actuator and the saturation temperature increase (Fig. 5b and c). Fig. S5a exhibits the optical view of bending angle of the soft actuator at different voltages. Blocking force of the MPDMS/MXene/PTFE soft actuator in this study was measured by contacting the edge of actuator with force sensor (Fig. 5d, red line). The detected force reached 33.35 mN at 3.0 V. Fig. S5b shows a time history of the blocked forces under dc fields between 1 and 3 V_{DC}. As time increase, the force increases and decreases after a maximum point. This was also ascribed to creep and relaxation in the MPDMS material. As shown in Fig. S5c, the bending angle of the actuator increases with the increase of applied voltage which indicates that the deformation of the soft actuator can be programmatically controlled. Additionally, the resistance of the actuator during bending process is steady, which demonstrates a high electrical stability of the soft actuator (Fig. S5d). According to the Joule heat formula $Q = U^2t/R$, as the input voltage increases, the soft actuator can convert more electric energy into thermal energy. The large thermal expansion coefficient between the MPDMS film and PTFE tape favors for a larger bending deformation in the soft actuator with the increase of saturation temperature. As shown in Fig. 5e and Video S1, when 2 V voltage is applied to the actuator, the actuator can respond quickly. With the passage of time, the deformation gradually enlarges, and a stable state is finally reached. Moreover, the deformation can maintain a stable state for a long time. Fig. 5f displays the temperature distribution and bending angle changes of the soft actuator under different voltages by using the infrared camera. As shown in the thermal images, the higher applied voltage leads to the higher temperature, and then the soft actuator exhibits a larger deformation. Typically, with a 3 V voltage, the actuator can generate a bending angle of 353°. The excellent ability of soft actuators to deform at low input voltages is due to three reasons. First, the high conductivity of MXene film results in a low driving voltage to achieve joule heating for electromechanical deformation of the actuator. Secondly, the significant difference of thermal expansion between PTFE tape and MPDMS film at elevated temperatures increases the crimping of the actuator, because the bending angle is proportional to the difference of thermal expansion coefficient. Finally, the soft and flexible nature of

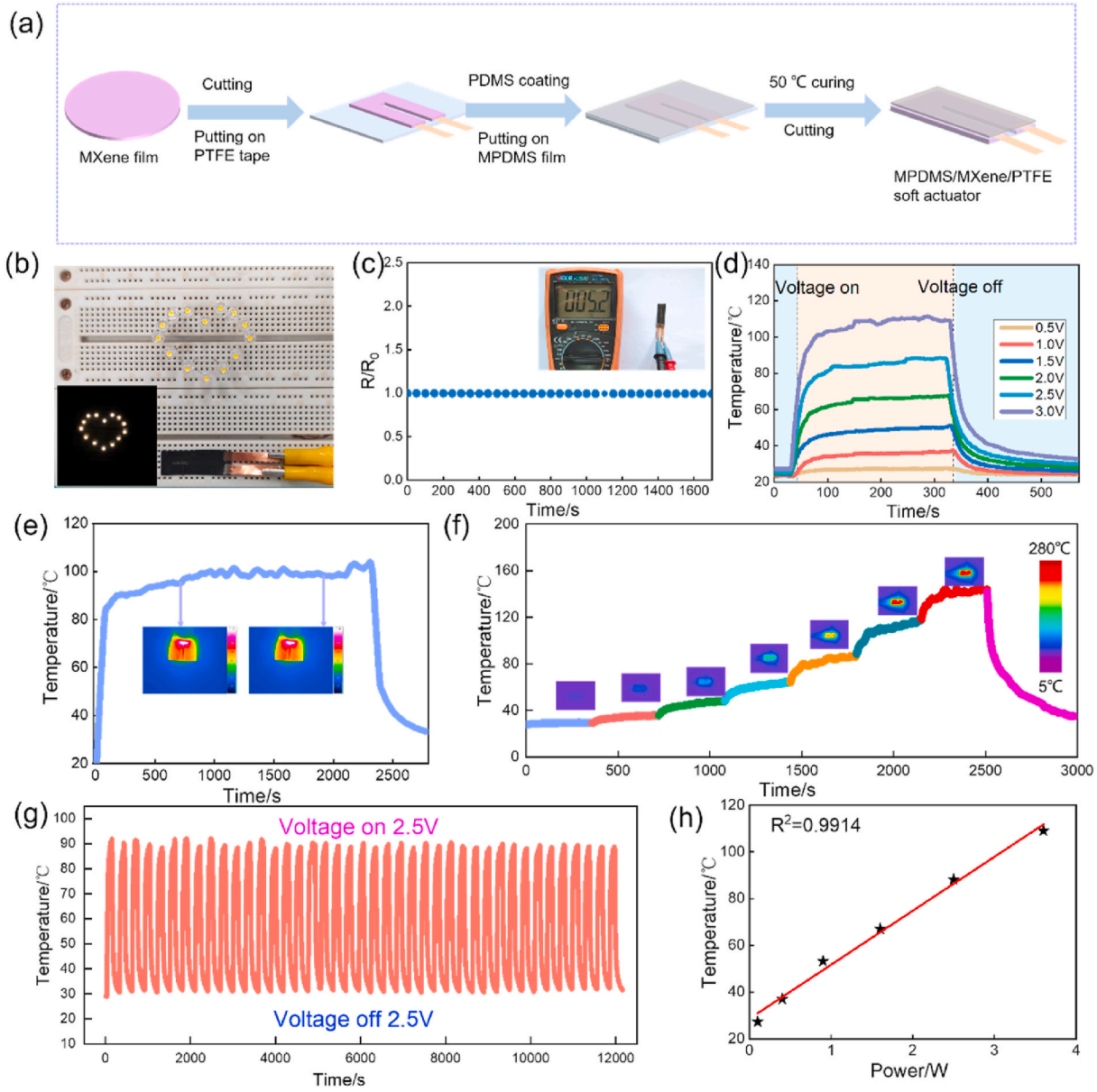

Fig. 4. Electrothermal performance of MPDMS/MXene/PTFE actuator. (a) Schematic illustration of the fabrication process of the MPDMS/MXene/PTFE soft actuator. (b) Lighting of the heart LED lamps *via* the MPDMS/MXene/PTFE actuator. (c) Real-time relative resistance of MPDMS/MXene/PTFE actuator. The resistance of the actuator is 5.2 Ω. (d) Time-dependent temperature profiles under different driving voltages for 300 s. (e) Temperature stability of MPDMS/MXene/PTFE actuator at a constant voltage of 2.5 V. (f) Temperature profiles upon dynamically supplied voltages from 0.5 to 3.5 V, insets are the corresponding infrared radiation (IR) thermal images of the actuator at different voltages. (g) Cyclic electrothermal stability of the actuator at 2.5 V voltage. (h) Experimental results of saturation temperature as a function of electrical power.

the material used in the actuator facilitates the deformation. Here, the performances of other previously reported actuators are consulted in Table S1. It is found that the MPDMS/MXene/PTFE actuator can reach about 110 °C at a voltage of 3 V and produce the bending angle of 353°.

3.3. *Intelligent hyperthermia insoles and thermal imaging arrays based on MPDMS/MXene/PTFE sandwich structure*

The excellent heating reliability, stability and repeatability make the MPDMS/MXene/PTFE sandwich structure have many applications in real life. Here, a wearable wear-resistant insole with hyperthermia function is fabricated based on the MPDMS/MXene/PTFE sandwich film (Fig. 6a and Fig. S6). Clinical experiments have proved that human feet are the epitome of the three-dimensional distribution of human organs and tissues. When the organs or glands in the body are abnormal, the corresponding foot reflex area will respond, such as pain, acid swelling and so on. Therefore, heating the specific foot reflection area can promote foot blood circulation, reduce local tension, effectively regulate the functions of various parts of the body, and enhance physique. By integrating the sandwich film units with a normal shoe, a thermal management device is obtained (Fig. 6d). The MPDMS/MXene/PTFE-based heating unit can quickly reach the desired temperature and the temperature can be kept stably, thus the MPDMS/MXene/PTFE-based heating unit can be implemented even if there is a long heating requirement. As shown in Fig. 6e, after 3 h continuous heating, the temperature has little fluctuation. Fig. 6b shows several important plantar reflex areas such as cephalic, cardiac, and gonad reflexes. By applying a voltage on MPDMS/MXene/PTFE sandwich films in different reflective areas, the reflective areas can be heated to relieve fatigue and pain. The infrared thermal imaging of MPDMS/MXene/PTFE-based unit

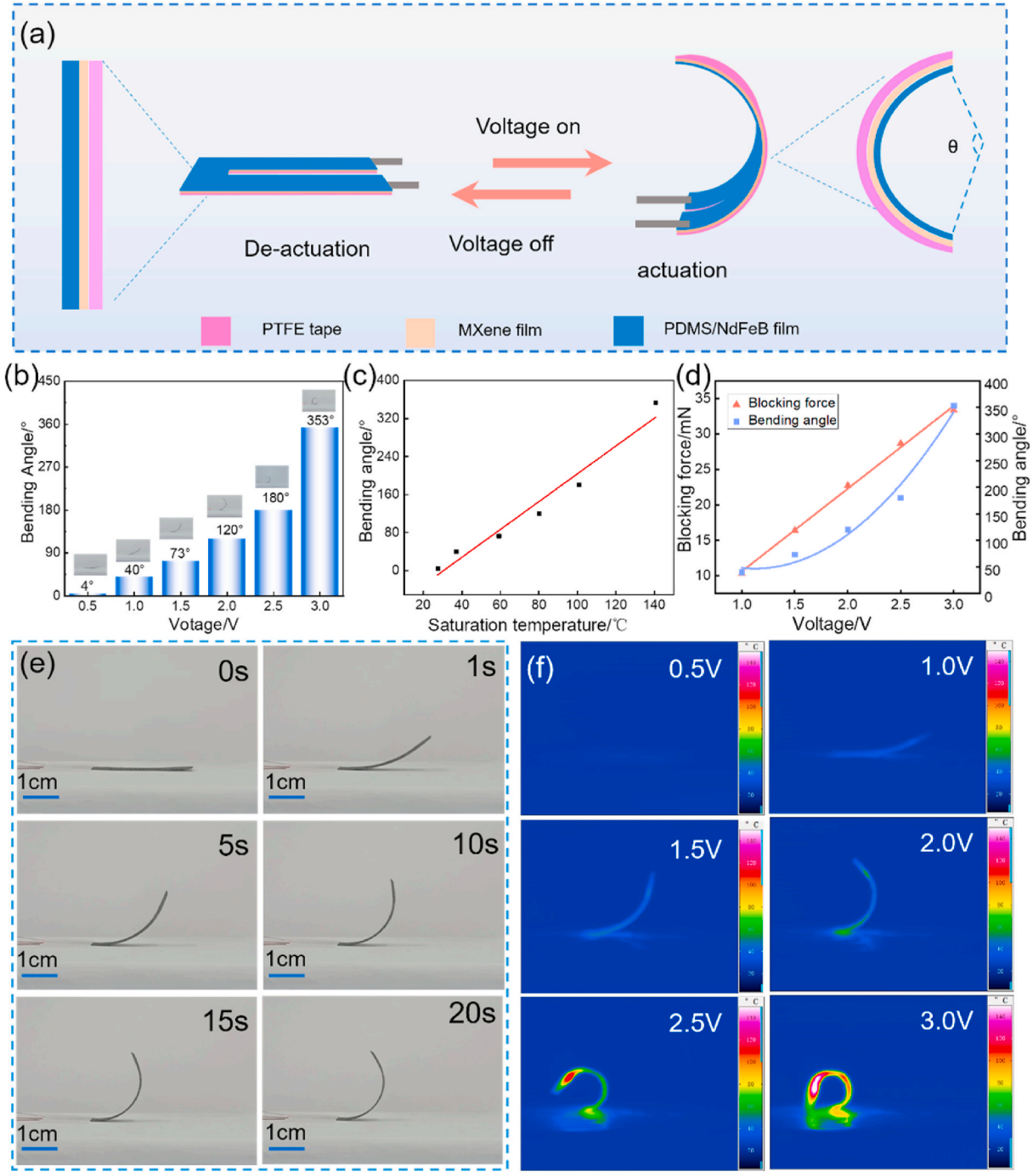

Fig. 5. The electrothermal-driven performance of the soft actuator. (a) Schematics of the actuator before/after actuation. (b) Bending angles as a function of different driving voltages. (c) The maximum bending angle of the actuator at different saturation temperatures. (d) Linear relationship between voltage and blocking forces (red line) and bending angle (blue line) of MPDMS/MXene/PTFE soft actuator. (e) Optical images of time-dependent electrothermal bending process for MPDMS/MXene/PTFE soft actuator under 2 V voltage. (f) IR images of the actuator under different voltages. (For interpretation of the references to color in this figure legend, the reader is referred to the Web version of this article.)

matrix also demonstrates the reflection areas are heated to the target temperature (Fig. 6c). As a result, the MPDMS/MXene/PTFE-based intelligent heat therapy insoles show broad application prospects in the field of human heat therapy.

In addition, based on the electrothermal performance of MPDMS/MXene/PTFE sandwich structure, the actuator is not only energized to generate heat, but also generate thermal radiation, thus it can be applied in the infrared thermal image due to its heating performance. Therefore, a flexible 5 × 5 heater array is fabricated with 25 units of 1 × 1 cm^2 (Fig. 6f). By connecting different elements in the matrix, it can display different information under the infrared thermal imager. In some special domains, MPDMS/MXene/PTFE sandwich structure can transmit information and Fig. 6g demonstrates the precise rendering of a matrix designed in the shape of "USTC" under an infrared camera.

3.4. MPDMS/MXene/PTFE-based intelligent gripper

Since the soft actuators have great potential in the control and

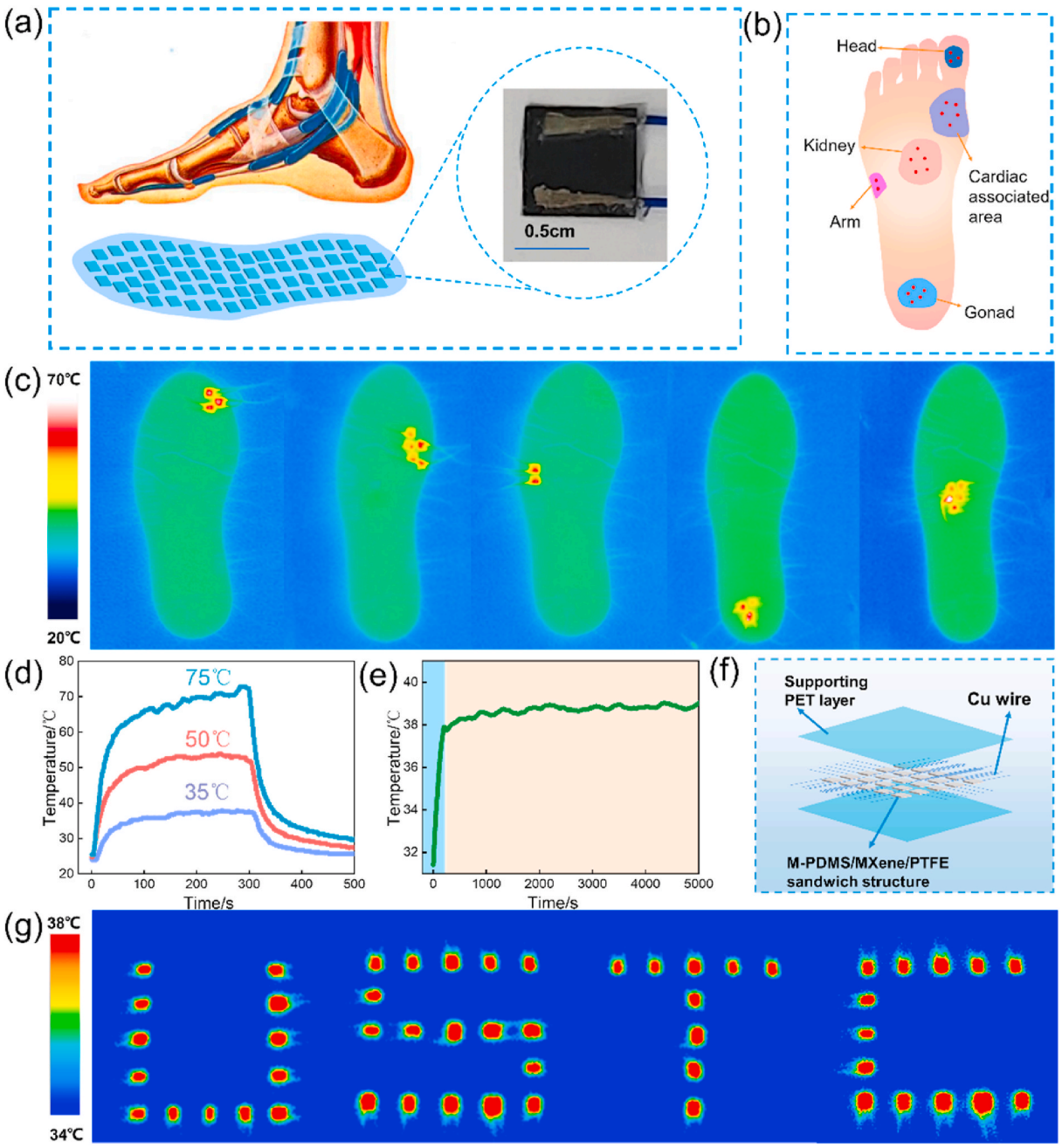

Fig. 6. (a) MPDMS/MXene/PTFE-based sole array on the shoe. Inset is an optical design of a heating unit. (b) Schematic showing the significant plantar reflection region. (c) Infrared thermal image of heating several important reflective areas of the plantar reflection region. (d) Time-dependent temperature profiles for heating the plantar reflection region at different temperatures for 300 s. (e) Temperature stability of heating the head reflection area. (f) Schematic of infrared display consisting of 5 × 5 arrays of MPDMS/MXene/PTFE sandwich structure and supporting PET layer. (g) Infrared picture of patterned heater array showing the letters "USTC".

transfer of items [45,46], a flexible intelligent four-fingered gripper is manufactured to study the feasibility of advanced structural actuators. Each finger (a MPDMS/MXene/PTFE actuator) is designed to be U-shaped so that it can be connected to a power supply. As shown in Fig. 7a, when a voltage is applied to the four-finger gripper, each finger deforms and pulls inward. After the voltage is turned off, all four fingers are restored to their original state simultaneously. Here, the process of grasping, transferring and releasing objects which imitating human gripper is studied. As shown in the Fig. 7b and Video S2, the four-finger actuator remains slightly bent down in its initial state under the action of gravity. When voltage is applied, four fingers grasp the bouquet of the fake flower (0.9242 g) tightly, and then move the bouquet to a high height without falling off under a stable voltage. Finally, turning off the voltage, all four fingers return to their original position. In addition, soft machines have proved to show great potential in the food processing industry. As shown in Fig. 7c, the four-finger actuator catches quail eggs when 3.5 V voltage is applied. It has been observed that the temperature of the actuator can reach 120 °C and quail eggs can be baked within 30 min. As shown in Fig. 7e, the baked quail eggs are darker than the common boiled quail eggs, suggesting that higher baking temperature than boiling water. The as-developed four-finger actuator can not only grab and transfer objects, but also effectively heat the captured objects, which proves that the soft actuator can be used for special scenes that require a single operation to achieve the transfer and heating of objects.

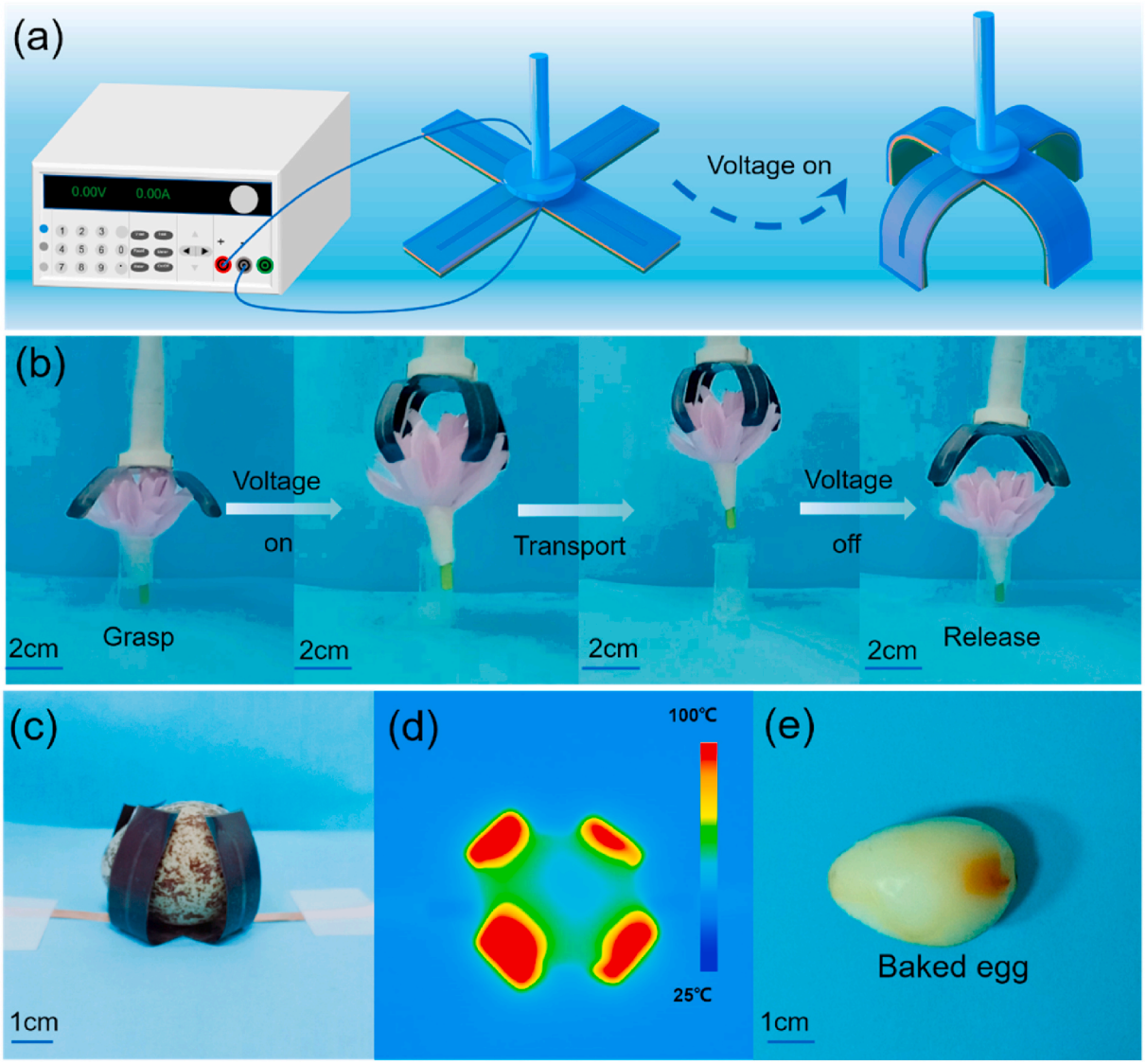

Fig. 7. (a) Working schematic diagram of the intelligent gripper based on MPDMS/MXene/PTFE soft actuator. (b) The intelligent gripper in the process of grabbing flower actuated by voltage drives. (c) Front view of the four-fingered actuator with four fingers wrapping around a quail egg and (d) the corresponding top-view of IR thermal image. (e) Photographs of quail eggs cooked by the four-fingered soft actuator.

3.5. Magnetic drive performance of MPDMS/MXene/PTFE actuator and the biomimetic dragonfly

The magnetic property plays an important role in determining the magneto-actuating characteristics of MPDMS/MXene/PTFE actuators. As shown in Fig. 8a and Fig. S7, one end of the MPDMS/MXene/PTFE actuator is fixed on the Tesla meter to measure its bending angle under different magnetic fields. Due to the presence of hard magnetic NbFeB particles, the magnetized MPDMS/MXene/PTFE actuator can be regarded as a permanent magnet, so it can achieve bidirectional bending under the magnetic field. As shown in Fig. 8b and c, the greater the applied magnetic field, the larger the bending angle of the MPDMS/MXene/PTFE actuator.

The MPDMS/MXene/PTFE soft actuator can be actuated by the magnetic field, hence it is used to design the biomimetic dragonfly wings and simulate the flapping behavior of dragonfly wings. Fig. 8e, f and g show the optical picture of the biomimetic dragonfly which flapping its wings in the magnetic field. As shown in the Video S3, the dragonfly actuator is centered over an electromagnet that provides a periodic magnetic field. After applying electric currents in different directions to the electromagnet, it generates different magnetic fields to attract and repel the wings of the dragonfly, thus mimicking the movement characteristics of dragonfly in nature. The dragonfly wings are in a plane state without the magnetic field. When the upward magnetic field is applied, the dragonfly wings and electromagnets repel each other, making the wings bend upward as a whole. When applying the downward magnetic field, dragonfly wings and electromagnets attract each other, making the wings bend downward. Furthermore, the deformation process of the biomimetic actuator can also be analyzed through Finite Element Method (FEM) (Fig. 8i, j and k). The trend between the simulation results and the measured deformation is consistent. It shows that the finite element analysis model can provide design guidance for the deformation process of bionic actuator with complex structure.

3.6. Intelligent crawling robot with electrothermal-magnetic coupling actuation

Self-walking is one of the basic motions of robots. As we all know, the inchworm (Fig. 9a) has a unique crawling pattern [47]. It first fixes the head, then pulls the tail forward to a certain extent, keeps the tail still, the head stretches forward, and finally releases it. Through the alternating movement of bending and stretching, the inchworm can move

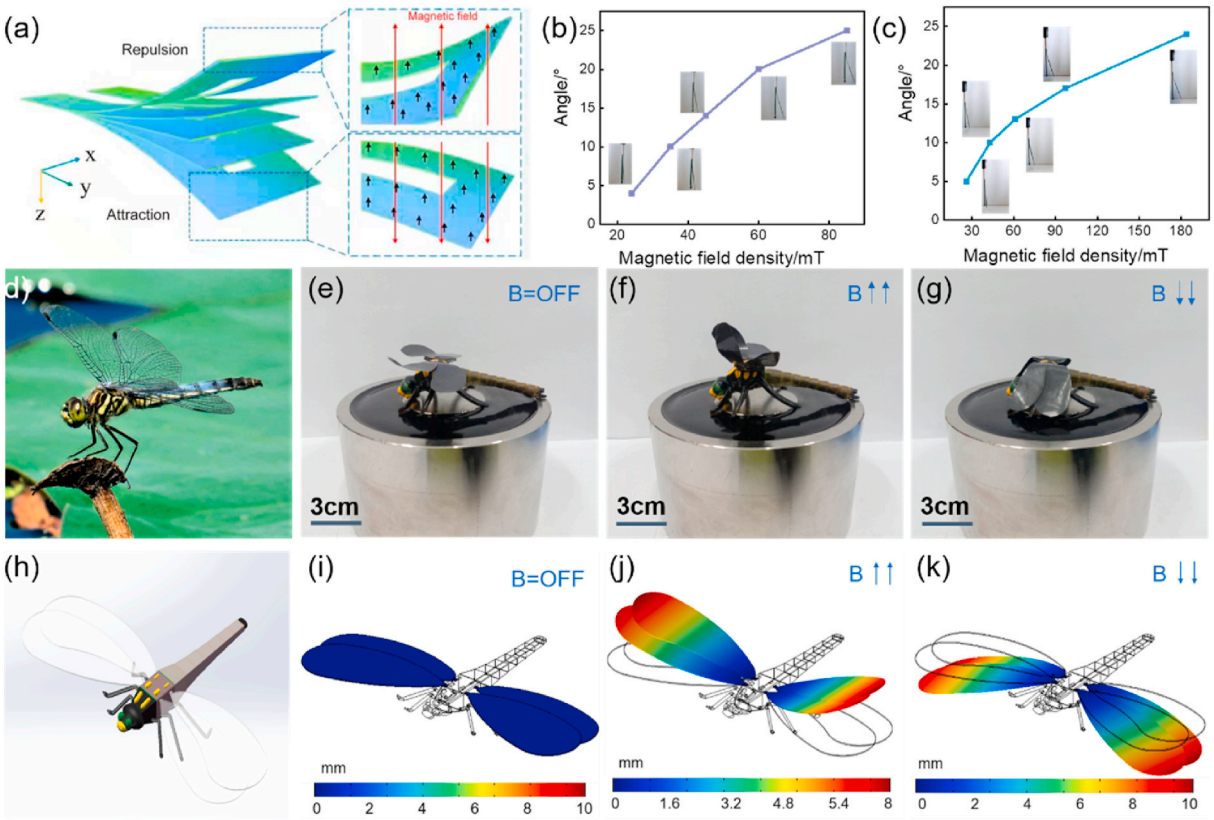

Fig. 8. (a) Schematic diagram of MPDMS/MXene/PTFE actuator bending under different magnetic field strength. Bending angle corresponding to different magnetic field intensity under the action of (b) attraction and (c) repulsion. (d) Optical image of a dragonfly resting on a lotus leaf. (e–g) Experimental magnetic actuation wings of bionic dragonfly on the leaves. (h) Dragonfly model for simulation. (i–k) Magnetically actuated flap motion of a bionic dragonfly analyzed by FEM.

directionally. By simulating this crawling principle, a worm-moving crawling biomimetic robot based on MPDMS/MXene/PTFE soft actuator is developed. The soft actuator is actuated with electrothermal stimuli first. The head and hail move closer on an asymmetrical surface structure when the voltage is applied and moved apart when the voltage is turned off. The asymmetrical surface structure is employed to promote one-directional walking motion (Fig. 9b and Video S4). However, the crawling robot cannot move forward on a flat surface only under electrothermal stimulation. As shown in the Fig. S8 and Videos S5 and S6, when a positive magnetic field was applied to the actuator during electrothermal bending, the actuator would be attracted or repelled by the magnetic field. Therefore, as long as the magnetic field in the appropriate direction was applied in the process of electrothermal driving, the effect of coupling driving could be achieved. As shown in the Fig. 9c and Video S7, we couple electrothermal and magnetic stimuli to accomplish the crawler robot moving forward in the plane. When the voltage is applied to the biomimetic robot, the head of the robot stays still, the tail shrinks inward and moves forward. However, only through the voltage control, the robot is difficult to climb forward, so a magnetic field is added under the robot for fixing the tail of the robot. After that, turn off the voltage, the tail of the robot is fixed, the head moves forward and returns to the flat state. Finally, the magnetic field is removed to realize the cyclic crawling motion of the soft robot. Under the action of external periodic magnetoelectric coupling, the robot can continuously crawl forward to achieve directional movement. The crawling robot demonstrated here can benefit the development of biomimetic robots that enable autonomous motions.

4. Conclusion

In summary, a novel multifunctional MPDMS/MXene/PTFE sandwich film with both electrothermal and magnetic-actuation performance was developed. Due to the excellent electrical conductivity of MXene film and the thermal expansion difference between the MPDMS and PTFE layers, the prepared MPDMS/MXene/PTFE soft actuator can generate stable heat and produce large and rapid bending deformation at low voltage. When stimulated by 3 V voltage, the bending angle of the actuator reaches to as high as 353°. Because of its excellent electrothermal actuation performance, the actuator can be used as a component to construct various intelligent devices for bionic motion, such as grasping and heating irregular objects, hand movement and crawling. Owing to the hard magnetic NdFeB particles, the MPDMS/MXene/PTFE actuator can be bent under the action of a magnetic field. In addition, by integrating the electrothermal and magnetic drive performance of MPDMS/MXene/PTFE soft actuator, a crawling robot is designed. The crawling robot can crawl forward under coupling the electric and magnetic drive. This study provides a new idea for the designation of high-performance multifunctional coupling-actuated soft actuators for various practical applications, such as intelligent devices, soft robots, wearable soft electronics, etc.

Author statement

Wenwen Li and **Min Sang:** Conceptualization, Investigation, Methodology, Visualization, Writing-original draft. **Shuai Liu**: Investigation, Writing-review & editing, Formal analysis. **Bochao Wang** and **Xufeng Cao:** Formal analysis. **Guanghui Liu:** Visualization. **Xinglong Gong:** Resources, Supervision, Project administration, Funding acquisition. **Lingyun Hao:** Conceptualization, Methodology. **Shouhu Xuan:** Methodology, Validation, Writing-review & editing, Funding acquisition.

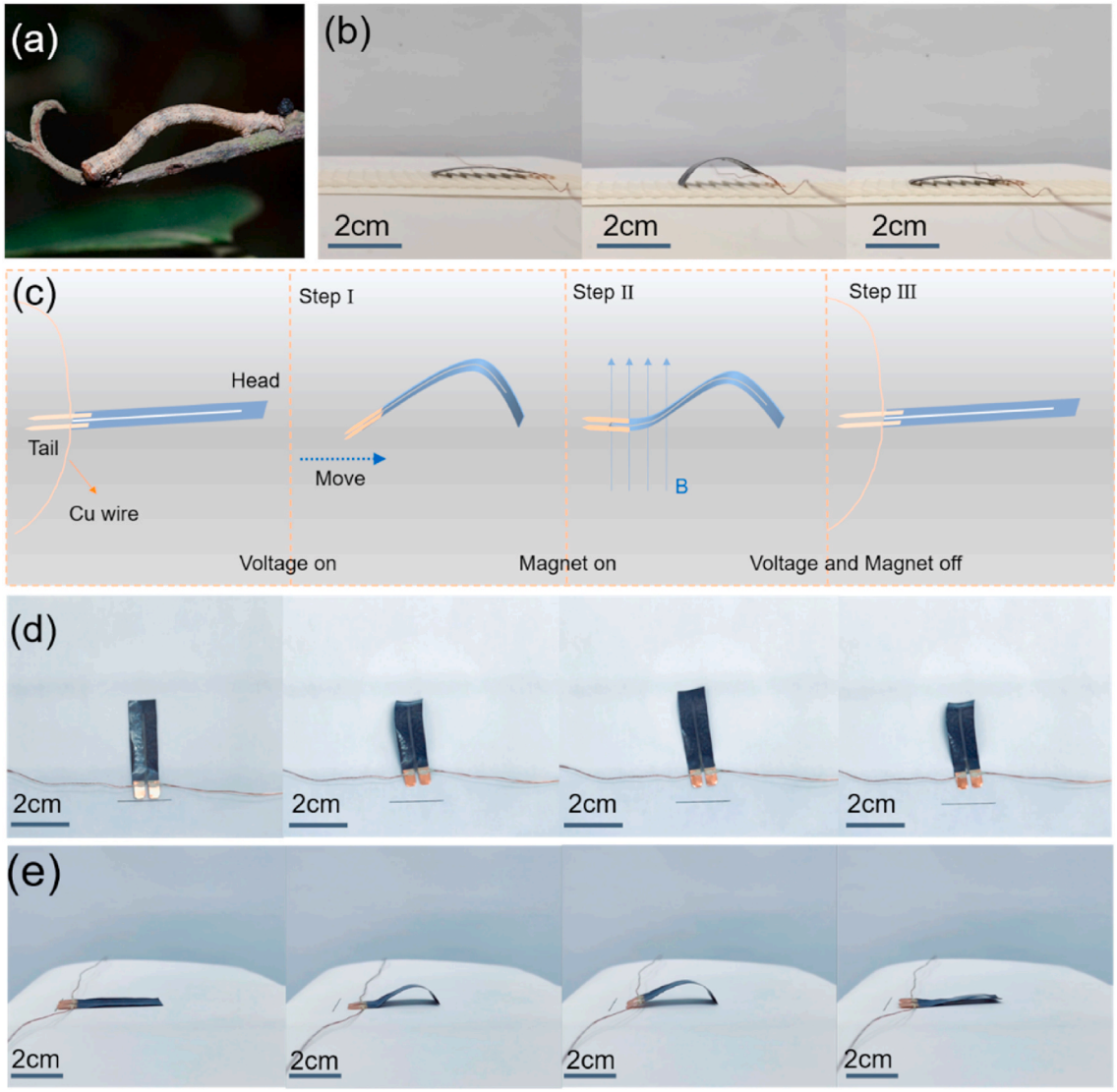

Fig. 9. (a) Optical image of the inchworm. (b) Consecutively captured images showing the U-shaped soft robot crawling on a flat ratchet surface when the voltage is periodically turned on and off. (c) Schematic design of a U-shaped soft robot with continuous directional crawling motion driven by electrothermal and magnetic coupling. (d) Optical top view and (e) side view of a U-shaped soft robot crawling controlled by the electrothermal and magnetic coupling effect.

Declaration of competing interest

The authors declare that they have no known competing financial interests or personal relationships that could have appeared to influence the work reported in this paper.

Acknowledgements

Financial supports from the National Natural Science Foundation of China (Grant Nos. 12072338, 11972343, 12132016), the Anhui's Key R&D Program of China (202104a05020009), the Fundamental Research Funds for the Central Universities (WK2480000007) and the Aviation Science Foundation of China (20200029079004), are gratefully acknowledged. This work was partially carried out at the USTC Center for Micro and Nanoscale Research and Fabrication.

Appendix A. Supplementary data

Supplementary data to this article can be found online at https://doi.org/10.1016/j.compositesb.2022.109880.

References

[1] Fusco S, Sakar MS, Kennedy S, Peters C, Bottani R, Starsich F, et al. An integrated microrobotic platform for on-demand, targeted therapeutic interventions. Adv Mater 2014;26(6):952–7.
[2] Yao SS, Cui JX, Cui Z, Zhu Y. Soft electrothermal actuators using silver nanowire heaters. Nanoscale 2017;9(11):3797–805.
[3] Mirvakili SM, Hunter IW. Artificial muscles: mechanisms, applications, and challenges. Adv Mater 2018;30(6):1704407.
[4] Ling Y, Pang WB, Li XP, Goswami S, Xu Z, Stroman D, et al. Laser-induced graphene for electrothermally controlled, mechanically guided, 3D assembly and human-soft actuators interaction. Adv Mater 2020;32(17):1908475.
[5] Huang Y, Hu W, Wang XL, Guo XH, Hao C, Zhao YN, et al. A low-voltage graphene/Ag-based PhaseTransition-controlled force actuator. Compos B Eng 2019;174:9.
[6] Feng JB, Xuan SH, Ding L, Gong XL. Magnetoactive eastomer/PVDF composite film based magnetically controllable sctuator with real-time deformation feedback property. Compos. Part A 2017;103:25–34.
[7] Wang Q, Wu ZH, Huang JY, Du ZL, Yue YM, Chen DZ, et al. Integration of sensing and shape-deforming capabilities for a bioinspired soft robot. Compos B Eng 2021;223:10.
[8] Wang ZB, Wu YG, Wu DZ, Sun DH, Lin LW. p soft magnetic composites for highly deformable actuators by four-dimensional electrohydrodynamic printing. Compos B Eng 2022;231:9.
[9] Yang LY, Cui J, Zhang L, Xu XR, Chen X, Sun DP. A moisture-driven actuator based on polydopamine-modified MXene/bacterial cellulose nanofiber composite film. Adv Funct Mater 2021;31(27):11.

[10] Sun YP, Hou KH, Zhang D, Chang SL, Ye L, Cao AY, et al. High performance carbon nanotube/polymer composite fibers and water-driven actuators. Compos Sci Technol 2021;206:108676.
[11] Taccola S, Greco F, Sinibaldi E, Mondini A, Mazzolai B, Mattoli V. Toward a new generation of electrically controllable hygromorphic soft actuators. Adv Mater 2015;27(10):1668.
[12] Kim H, Kang JH, Zhou Y, Kuenstler AS, Kim Y, Chen C, et al. Light-driven shape morphing, assembly, and motion of nanocomposite gel surfers. Adv Mater 2019;31(27):1900932.
[13] Qi XD, Shao YW, Wu HY, Yang JH, Wang Y. Flexible phase change composite materials with simultaneous light energy storage and light-actuated shape memory capability. Compos Sci Technol 2019;181:107714.1–9.
[14] Luo XJ, Li LL, Zhang HB, Zhao S, Zhang Y, Chen W, et al. Multifunctional $Ti_3C_2T_x$ MXene/low-density polyethylene soft robots with programmable configuration for amphibious motions. ACS Appl Mater Interfaces 2021;13(38):45833–42.
[15] Chen LZ, Weng MC, Zhou ZW, Zhou Y, Zhang LL, Li JX, et al. Large-deformation curling actuators based on carbon nanotube composite: advanced-structure design and biomimetic application. ACS Nano 2015;9(12):12189–96.
[16] Chen LZ, Liu CH, Liu K, Meng CZ, Hu CH, Wang JP, et al. High-performance, low-voltage, and easy-operable bending actuator based on aligned carbon nanotube/polymer composites. ACS Nano 2011;5(3):1588–93.
[17] Sang M, Liu GH, Liu S, Wu YX, Xuan SH, Wang S, et al. Flexible PTFE/MXene/PI soft electrothermal actuator with electromagnetic-interference shielding property. Chem Eng J 2021;414:128883.
[18] Hu Y, Liu JQ, Chang LF, Yang LL, Xu AF, Qi K, et al. Electrically and sunlight-driven actuator with versatile biomimetic motions based on rolled carbon nanotube bilayer composite. Adv Funct Mater 2017;27(44):1704388.
[19] Chen LZ, Weng MC, Zhou PD, Zhang LL, Huang ZG, Zhang W. Multi-responsive actuators based on A graphene oxide composite: intelligent robot and bioinspired applications. Nanoscale 2017;9(28):9825–33.
[20] Li LL, Zhao S, Luo XJ, Zhang HB, Yu ZZ. Smart MXene-based Janus films with multi-responsive actuation capability and high electromagnetic interference shielding performances. Carbon 2021;175:594–602.
[21] Hu Y, Chen W, Lu LH, Liu JH, Chang CR. Electromechanical actuation with controllable motion based on a single-walled carbon nanotube and natural biopolymer composite. ACS Nano 2010;4(6):3498–502.
[22] Fan HW, Li KR, Li Q, Hou CY, Zhang QH, Li YG, et al. Prepolymerization-assisted fabrication of an ultrathin immobilized layer to realize A semi-embedded wrinkled AgNW network for A smart electrothermal chromatic display and actuator. J Mater Chem C 2017;5(37):9778–85.
[23] Lee H, Kim H, Ha I, Jung J, Won P, Cho H, et al. Directional shape morphing transparent walking soft robot. Soft Robot 2019;6(6):760–7.
[24] Kim H, Lee H, Ha I, Jung J, Won P, Cho H, et al. Biomimetic color changing anisotropic soft actuators with integrated metal nanowire percolation network transparent heaters for soft robotics. Adv Funct Mater 2018;28(32):1801847.1–8.
[25] Hu Y, Xu AF, Liu JQ, Yang LL, Chang LF, Huang MJ, et al. Multifunctional soft actuators based on anisotropic paper/polymer bilayer toward bioinspired applications. Adv Mater Technol-UA 2019;4(3):1800674.
[26] Liu J, Liu ZS, Zhang HB, Chen W, Zhao ZF, Wang QW, et al. Ultrastrong and highly conductive MXene-based films for high-performance electromagnetic interference shielding. Adv Electron Mater 2020;6(1):1901094.
[27] Fan HW, Li KR, Li Q, Hou CY, Zhang QH, Li YG, et al. Prepolymerization-assisted fabrication of an ultrathin immobilized layer to realize a semi-embedded wrinkled AgNW network for a smart electrothermal chromatic display and actuator. J Mater Chem C 2017;5(37):9778–85.
[28] Luo JQ, Zhao S, Zhang HB, Deng ZM, Li LL, Yu ZZ. Flexible, stretchable and electrically conductive MXene/natural rubber nanocomposite films for efficient electromagnetic interference shielding. Compos Sci Technol 2019;182:107754.1–8.
[29] Song DK, Li XF, Li XP, Jia XQ, Min P, Yu ZZ. Hollow-structured MXene-PDMS composites as flexible, wearable and highly bendable sensors with wide working range. J Colloid Interface Sci 2019;555:751–8.
[30] Chen W, Liu LX, Zhang HB, Yu ZZ. Kirigami-inspired highly stretchable, conductive, and hierarchical $Ti_3C_2T_x$ MXene films for efficient electromagnetic interference shielding and pressure sensing. ACS Nano 2021;15(4):7668–81.
[31] Umrao S, Tabassian R, Kim J, Nguyen V, Zhou QT, Nam S, et al. MXene artificial muscles based on ionically cross-linked $Ti_3C_2T_x$ electrode for kinetic soft robotics. Sci Robot 2019;4(33):7797.
[32] Liu WJ, Cheng YF, Liu NS, Yue Y, Lei DD, Su TY, et al. Bionic MXene actuator with multiresponsive modes. Chem Eng J 2021;417:129288.
[33] Dong Y, Wang J, Guo XK, Yang SS, Ozen MO, Chen P, et al. Multi-stimuli-responsive programmable biomimetic actuator. Nat Commun 2019;10:4087.
[34] Yang LL, Qi K, Chang LF, Xu AF, Hu Y, Zhai H, et al. A powerful dual-responsive soft actuator and photo-to-electric generator based on graphene micro-gasbags for bioinspired applications. J Mater Chem B 2018;6(31):5031–8.
[35] Zhang QC, Wang MA, Ao HY, Luo HL, Deng XY, Wan YZ. Embedding carbon nanotube to the surfaces of poly(epsilon-caprolactone) film for multi-responsive actuations. Polym Test 2021;96:1070086.
[36] Won S, Kim S, Park JE, Jeon J, Wie JJ. On-demand orbital maneuver of multiple soft robots via hierarchical magnetomotility. Nat Commun 2019;10:4751.
[37] Jiralerspong T, Bae G, Lee JH, Kim SK. Wireless control of two- and three-dimensional actuations of kirigami patterns composed of magnetic-particles-polymer composites. ACS Nano 2020;14(12):17589–96.
[38] Kim Y, Yuk H, Zhao RK, Chester SA, Zhao XH. Printing ferromagnetic domains for untethered fast-transforming soft materials. Nature 2018;558(7709):274–9.
[39] Kim Y, Parada GA, Liu SD, Zhao XH. Ferromagnetic soft continuum robots. Sci Robot 2019;4(33):7329.
[40] Schmidt AM. Electromagnetic activation of shape memory polymer networks containing magnetic nanoparticles. Macromol Rapid Commun 2006;27(14):1168–72.
[41] Ze QJ, Kuang X, Wu S, Wong J, Montgomery SM, Zhang RD, et al. Magnetic shape memory polymers with integrated multifunctional shape manipulation. Adv Mater 2020;32(4):1906657.
[42] Uh K, Yoon B, Lee CW, Kim JM. An electrolyte-free conducting polymer actuator that displays electrothermal bending and flapping wing motions under a magnetic field. ACS Appl Mater Interfaces 2016;8(2):1289–96.
[43] Zhang W, Ahmed S, Masters S, Ounaies Z, Frecker M. Finite element analysis of electroactive polymer and magnetoactive elastomer based actuation for Origami folding. Smart Mater Struct 2017;26(10):105032.
[44] Shahzad F, Alhabeb M, Hatter CB, Anasori B, Hong SM, Koo CM, et al. Electromagnetic interference shielding with 2D transition metal carbides (MXenes). Science 2016;353(6304):1137–40.
[45] Amjadi M, Sitti M. High-performance multiresponsive paper actuators. ACS Nano 2016;10(11):10202–10.
[46] Ma B, Xu CT, Cui LS, Zhao C, Liu H. Magnetic printing of liquid metal for perceptive soft actuators with embodied intelligence. ACS Appl Mater Interfaces 2021;13(4):5574–82.
[47] Ahn CY, Liang XD, Cai SQ. Bioinspired design of light-powered crawling, squeezing, and jumping untethered soft robot. Adv Mater Technol 2019;4(7):1900185.